European Journal of Physics

PAPER

A non-traditional fluid problem: transition between theoretical models from Stokes' to turbulent flow

To cite this article: Horacio D Salomone *et al* 2018 *Eur. J. Phys.* **39** 035002

IOP Publishing European Journal of Physics
Eur. J. Phys. **39** (2018) 035002 (16pp) https://doi.org/10.1088/1361-6404/aaa34b

A non-traditional fluid problem: transition between theoretical models from Stokes' to turbulent flow

Horacio D Salomone[1,3], **Néstor A Olivieri**[1], **Maximiliano E Véliz**[1] and **Lisandro A Raviola**[1,2]

[1] Instituto de Industria, Universidad Nacional de General Sarmiento. Juan María Gutiérrez 1150, (B1613GSX) Los Polvorines, Buenos Aires, Argentina
[2] Instituto de Educación, Universidad Nacional de Hurlingham. Teniente Manuel Origone 151, (B1688AXC) Villa Tesei, Buenos Aires, Argentina

E-mail: hsalomon@ungs.edu.ar and lraviola@ungs.edu.ar

Received 7 September 2017, revised 6 December 2017
Accepted for publication 20 December 2017
Published 9 March 2018

Abstract
In the context of fluid mechanics courses, it is customary to consider the problem of a sphere falling under the action of gravity inside a viscous fluid. Under suitable assumptions, this phenomenon can be modelled using Stokes' law and is routinely reproduced in teaching laboratories to determine terminal velocities and fluid viscosities. In many cases, however, the measured physical quantities show important deviations with respect to the predictions deduced from the simple Stokes' model, and the causes of these apparent 'anomalies' (for example, whether the flow is laminar or turbulent) are seldom discussed in the classroom. On the other hand, there are various variable-mass problems that students tackle during elementary mechanics courses and which are discussed in many textbooks. In this work, we combine both kinds of problems and analyse—both theoretically and experimentally—the evolution of a system composed of a sphere pulled by a chain of variable length inside a tube filled with water. We investigate the effects of different forces acting on the system such as weight, buoyancy, viscous friction and drag force. By means of a sequence of mathematical models of increasing complexity, we obtain a progressive fit that accounts for the experimental data. The contrast between the various models exposes the strengths and weaknessess of each one. The proposed experience can be useful for integrating concepts of elementary mechanics and fluids, and is suitable as laboratory practice, stressing the importance of the experimental validation of theoretical models and showing the model-building processes in a didactic framework.

[3] Author to whom any correspondence should be addressed.

Keywords: variable mass, fluid mechanics, drag coefficient, Stokes' law, laboratory practice

(Some figures may appear in colour only in the online journal)

1. Introduction

Fluid mechanics is a complex subject, and as such its teaching presents great challenges for both teachers and students, even in early university courses. Commonly used textbooks assume many simplifying hypotheses (incompressible fluid, ideal fluid, Newtonian fluid, laminar flow, etc) in order to develop approximate models to make phenomena in this domain more amenable to analytical treatment. As an important example of this approach, we have the deceptively simple *Stokes' law* [1–3],

$$\mathbf{F}_{\rm r} = -6\pi\eta r\mathbf{v}, \tag{1}$$

that models the relationship between the velocity $\mathbf{v}$ of a sphere of radius r and the drag force $\mathbf{F}_{\rm r}$ exerted on it by a viscous fluid with dynamical vicosity η. This equation was devised in 1851 by George Gabriel Stokes for incompressible Newtonian fluids in the limit of very low Reynolds' numbers Re, a situation in which the inertial forces are negligible in comparison with viscous forces [4]. This usually happens when the velocity is low, the viscosity is very large, and the length-scale of the flow is very small, giving rise to a laminar flow. Despite its simplicity, the scientific relevance of this result cannot be underestimated, remembering for example that Millikan used a slightly modified form of this equation in his famous oil-drop experiment to determine the electron charge (see article [5] and references therein). Besides, this law has technological importance as it is routinely applied to measure fluids viscosity in research and industrial laboratories by means of a device called a *falling-sphere viscometer* [1, 6]. In teaching laboratories, a similar device is used to show that the motion of a ball falling through a high viscosity fluid like glycerin attains a *terminal velocity*, and to determine the fluid viscosity by means of Stokes' and Archimedes' laws [7]. However, straightforward application of Stokes' law without a previous discussion of its applicability domain and a careful analysis of the actual experimental conditions can lead students to erroneous conclusions, as many previous works have pointed out [7–14].

In this work, we investigate a variation of the standard Stokes' problem, attaching to the sphere a chain which pulls it downwards with a length-dependent force (see figure 1). As the chain falls, it exerts a variable force on the sphere, mimicking the behaviour of a variable-mass system. With the aim of investigating this problem from an integrating approach (theoretical, computational and experimental), and to make explicit the model construction process in a didactic context, we propose a sequence of mathematical models of increasing complexity and compare its predictions to experimental observations. With this purpose, we divided the analysis in various stages which students can address sequentially under the form of various laboratory activities. To gain some intuition about the system and to understand the logic behind the process, we first consider the motion of the sphere without the chain. Afterwards, the full sphere-and-chain system is analyzed in a similar fashion.

2. Theoretical considerations

In the present section, we develop a series of theoretical models that will be contrasted against the experimental data obtained with the device introduced in the next section. We begin by

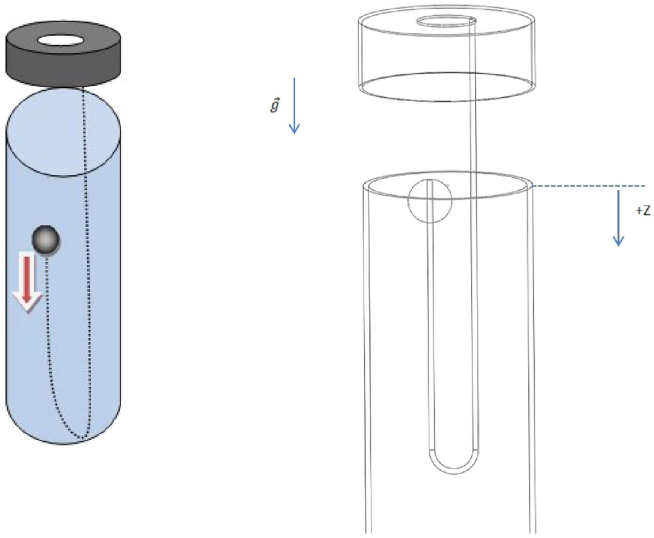

Figure 1. Schematic representation of the problem, showing the cylindrical fluid container, the falling sphere and the chain hanging from it.

investigating the motion of the sphere alone and then we study the effect of adding the chain to the system. In both cases, only the vertical component of the motion is taken into account, in spite of the fact that there exist a minor lateral displacement[4].

2.1. Sphere falling inside a stationary fluid under the action of gravity

Model 1 (viscous friction). As a first approximation to the problem we analyse the classical Stokes' model, considering a sphere of mass m and radius r falling inside a stationary fluid with density ρ and dynamical viscosity η. The mathematical model for the sphere's motion stems from Newton's second law and is given by the following equation:

$$m\frac{\mathrm{d}^2 z}{\mathrm{d}t^2} = W - B - F_{\mathrm{r}}, \tag{2}$$

$$= mg - \frac{4}{3}\pi\rho r^3 g - 6\pi\eta r\,\frac{\mathrm{d}z}{\mathrm{d}t}, \tag{3}$$

$$= \left(m - \frac{4}{3}\pi\rho r^3\right)g - B_1\,\frac{\mathrm{d}z}{\mathrm{d}t}, \tag{4}$$

where $W = mg$ is the sphere's weight, B is the buoyant force given by Archimedes' principle and

$$F_{\mathrm{r}} = 6\pi\eta r\frac{\mathrm{d}z}{\mathrm{d}t} = B_1\frac{\mathrm{d}z}{\mathrm{d}t} \tag{5}$$

[4] We disregard this oscillating horizontal motion as our measurements show that in the worst case the horizontal speed is at most a quarter of the vertical one, and it is usually much less than that. However, the combination of vertical and horizontal motion gives rise to a helical trajectory which can be observed and has already been reported in the literature [15].

is the viscous force proportional to velocity from Stokes' law. In our reference frame, the z axis points vertically downwards, as indicated in figure 1.

Model 2 (viscous friction and edge effect correction). Since the sphere is moving inside a tube of finite extent, its walls can cause a non-negligible edge effect. This effect was not considered in the original Stokes' derivation, who deduced its formula for an infinite fluid. Ladenburg, among others, analized the influence of a cylindrical container geometry and proposed the following correction factor to Stokes' law:

$$\gamma = \frac{1 - 3.3\left(\frac{r}{h}\right) - \dots}{1 - 2.104\left(\frac{r}{R}\right) - 2.09\left(\frac{r}{R}\right)^3 - \dots}, \tag{6}$$

where R is the radius of the container and h its height [16, 17]. The corrected viscous force is then given by $F_\mathrm{r} = \gamma B_1 \frac{\mathrm{d}z}{\mathrm{d}t}$. The equation of motion (2) with Ladenburg's correction factor is given by

$$m\frac{\mathrm{d}^2 z}{\mathrm{d}t^2} = \left(m - \frac{4}{3}\pi\rho r^3\right)g - \gamma B_1\frac{\mathrm{d}z}{\mathrm{d}t}. \tag{7}$$

Model 3 (drag force, constant drag coefficient). As previously said, Stokes' law is valid for laminar flows, i.e. for fluid motion with very low Reynolds' number Re. This number can be determined according to the expression [1–3]

$$Re = \frac{2\rho r v}{\eta}. \tag{8}$$

If the condition $Re < 1$ is not fulfilled, it is not expected that the Stokes' law will be valid. Also, when a sphere moves inside a viscous fluid, turbulent flow usually arises for $Re \approxeq 10^3$. In the experiments we performed with the sphere, terminal velocities ranging from 0.1 to 0.325 $\mathrm{m\,s^{-1}}$ were measured (see section 4). Then the Reynolds' number range for our experiments was

$$3.7 \times 10^3 < Re < 1.21 \times 10^4 \tag{9}$$

so we can assert that the flow regime for the falling sphere is transitioning to turbulent. This case cannot be accounted for by means of models 1 and 2, as the experimental results of the following sections will reveal.

Beyond the laminar regime, the validity of the Stokes' law breaks down and we have to recourse to more sophisticated—mostly empirical—models. These models are usually written in the form

$$F_\mathrm{r} = \frac{1}{2}C_\mathrm{D}\rho A v^2, \tag{10}$$

where A is the cross-sectional area of the object perpendicular to the direction of flow ($A = \pi r^2$ for a sphere) and C_D is a nondimensional *drag coefficient* which generally depends on many factors, most notably the shape of the body, the Reynolds number of the flow, the surface roughness, and the influence of neighbouring bodies or surfaces [2, 3]. In the case of a perfect sphere, the drag coefficient C_D depends exclusively on the Reynolds' number and is given with high precision by the empirical relation [2]

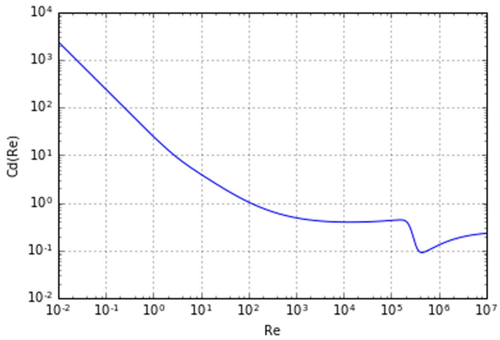

Figure 2. Drag coefficient C_D as a function of the Reynolds' number Re for a sphere, as given by the empirical formula (11). In the range $10^3 < Re < 10^5$, the drag coefficient is approximately constant ($C_D \approxeq 0.4$), a fact which is exploited in *model 3,* equations (12) and (25). The full relation is used in *model 4*, equations (13) and (26).

$$C_D(Re) = \frac{24}{Re} + \frac{2.6\left(\frac{Re}{5.0}\right)}{1 + \left(\frac{Re}{5.0}\right)^{1.52}} + \frac{0.411\left(\frac{Re}{2.63 \times 10^5}\right)^{-7.94}}{1 + \left(\frac{Re}{2.63 \times 10^5}\right)^{-8.00}} + \frac{0.25\left(\frac{Re}{10^6}\right)}{1 + \left(\frac{Re}{10^6}\right)} \tag{11}$$

whose graph is shown in figure 2. A straightforward calculation shows that for $Re \rightarrow 0$ we recover Stokes' law.

Figure 2 reveals that for values of Re ranging from 10^3 to 10^5 the drag coefficient is reasonably well approximated by the value $C_D \approxeq 0.4$. Using this value and subtituting equation (10) into (2), we arrive at the following equation of motion:

$$m\frac{d^2z}{dt^2} = mg - \frac{4}{3}\pi\rho r^3 g - 0.2\ \rho\pi r^2\left(\frac{dz}{dt}\right)^2 \qquad (10^3 < Re < 10^5). \tag{12}$$

Model 4 (drag force, variable drag coefficient). Finally, the equation of motion for the falling sphere in the non-laminar regime considering the dependence of C_D on the entire range of Re (equation (11)) is given by

$$m\frac{d^2z}{dt^2} = mg - \frac{4}{3}\pi\rho r^3 g - \frac{1}{2}C_D(Re)\ \rho\pi r^2\left(\frac{dz}{dt}\right)^2. \tag{13}$$

2.2. Sphere falling inside a fluid and pulled by a chain of variable length

By including the chain in the system, we must consider the new forces associated with it, such as its weight, the buoyancy force and the drag exerted by the fluid (see figure 3). These forces are dependent on the chain's length. If D_C is the chain diameter and L its initial length, the buoyancy force acting over it is

$$B_C = \rho\frac{\pi}{4}D_C^2(L - z)g \tag{14}$$

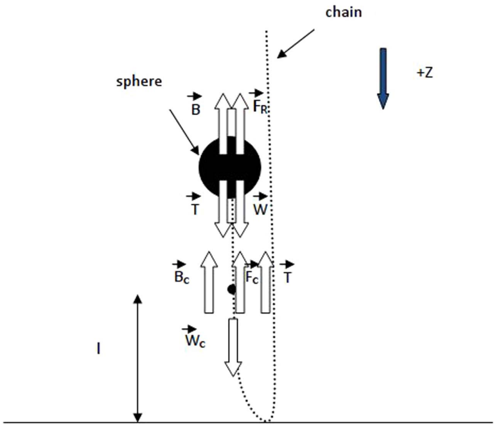

Figure 3. Schematic representation of the system investigated (sphere + chain), showing the forces acting on each body and the reference frame used. The z axis points vertically downwards and $z = 0$ at the top of the cylindrical container (not shown, for the actual experimental device see section 3).

and its weight is given by

$$W_C = \lambda(L - z)g, \tag{15}$$

where λ is the chain's linear mass density and z is the sphere's position measured from the top of the fluid container. Also, we must take into account the geometrical constraint that maintains the link between the two bodies. The chain exerts on the sphere a force T acting downwards, and the opposite force is acting over the chain by virtue of Newton's third law. If we consider the sphere as a point particle, its equation of motion is given by

$$ma = m\frac{d^2z}{dt^2} = T + W - B - F_r. \tag{16}$$

The equation of motion for the chain stems from the linear momentum balance equation

$$m_C a_C = \lambda(L - z)a_C = -T + W_C - B_C - F_C, \tag{17}$$

where m_C is the chain mass and a_C its centre-of-mass acceleration. This acceleration can be related to the sphere's acceleration by means of the constraint equation

$$z_C = z + \frac{l}{2} = z + \frac{L - z}{2} = \frac{1}{2}(L + z) \tag{18}$$

such that

$$a_C = \ddot{z}_C = \frac{1}{2}\ddot{z}. \tag{19}$$

Introducing equation (19) in (17) and adding (16) to (17), we arrive at the following equation of motion for the system:

$$\left(m + \frac{1}{2}\lambda(L - z)\right)\frac{d^2z}{dt^2} = (\overbrace{W + W_C}^{\text{Weight}}) - (\overbrace{B + B_C}^{\text{Buoyancy}}) - (\overbrace{F_r + F_C}^{\text{friction/drag}}) \tag{20}$$

$$= \left[m + \left(\lambda - \rho\frac{\pi}{4}D_{\mathrm{C}}^{2}\right)(L - z) - \frac{4}{3}\pi\rho r^{3}\right]g - (F_{\mathrm{r}} + F_{\mathrm{C}}). \tag{21}$$

It is worth noting that the factor accompanying the acceleration term—the system mass—depends on the chain length. Thus, we are addressing a variable mass problem, as previously stated.

In what follows, we will widen the analysis of the previous subsection by considering four models with different drag forces acting on the sphere and the chain.

Model 1 (viscous friction). Analogously to the case of the single sphere, we propose as a first approximation a viscous force acting on the chain—proportional to both speed and chain length—given by

$$F_{\mathrm{C}} = B_{2}(L - z)\frac{\mathrm{d}z}{\mathrm{d}t}, \tag{22}$$

where B_2 is a constant coefficient of viscous friction per unit length. This coefficient is a free parameter of the model that must be experimentally adjusted. For the sphere we maintain the viscous force given by equation (5). Hence, the equation of motion associated to this model is

$$\left(m + \frac{1}{2}\lambda(L - z)\right)\frac{\mathrm{d}^{2}z}{\mathrm{d}t^{2}} = \left[m + \left(\lambda - \rho\frac{\pi}{4}D_{\mathrm{C}}^{2}\right)(L - z) - \frac{4}{3}\pi\rho r^{3}\right] \times g - (B_{1} + B_{2}(L - z))\frac{\mathrm{d}z}{\mathrm{d}t}. \tag{23}$$

Model 2 (viscous friction and edge effect correction). As a second step, we take into account the Ladenburg edge effect correction for the sphere [13]. However, we retain for the chain the previous coefficient B_1 since we consider that the edge effect on it is negligible when compared to that of the sphere, as a consequence of its lower cross-sectional area (this effectively amounts to consider the chain as an infinitely thin wire). Therefore, the model can be expressed as follows:

$$\left(m + \frac{1}{2}\lambda(L - z)\right)\frac{\mathrm{d}^{2}z}{\mathrm{d}t^{2}} = \left[m + \left(\lambda - \rho\frac{\pi}{4}D_{\mathrm{C}}^{2}\right)(L - z) - \frac{4}{3}\pi\rho r^{3}\right] \times g - (\gamma\, B_{1} + B_{2}(L - z))\frac{\mathrm{d}z}{\mathrm{d}t}. \tag{24}$$

Model 3 (drag force with constant coefficient). Recalling model 3 for the single sphere, we now consider the regime in which the fluid motion is developing a turbulent behaviour, whereby viscous friction forces become negligible with respect to drag forces [13]. In this case, a fixed drag coefficient $C_{\mathrm{D}} = 0.4$ is proposed for the drag force on the sphere according to our measured values of Re (see figure 2 and section 4). On the other hand, we assume for the chain a drag force analogous to the one acting on the sphere, with a constant drag coefficient B_{2a} (another free parameter to be determined experimentally), which in this case depends not only on the velocity squared but also on the chain's length . These considerations lead to the following equation of motion:

$$\left(m + \frac{1}{2}\lambda(L - z)\right)\frac{d^2z}{dt^2} = \left[m + \left(\lambda - \rho\frac{\pi}{4}D_C^2\right)(L - z) - \frac{4}{3}\pi\rho r^3\right] \times g - (0.2 + B_{2a}(L - z))\left(\frac{dz}{dt}\right)^2. \quad (25)$$

Model 4 (drag force with variable drag coefficient). Our last model considers a variable drag coefficient for the sphere, which depends on Re as given by equation (11) (thus relaxing the condition $C_D = 0.4$), maintaining for the chain the same drag force of the previous model. The full model is represented by the equation

$$\left(m + \frac{1}{2}\lambda(L - z)\right)\frac{d^2z}{dt^2} = \left[m + \left(\lambda - \rho\frac{\pi}{4}D_C^2\right)(L - z) - \frac{4}{3}\pi\rho r^3\right] \times g - \left(\frac{1}{2}C_D(Re)\rho A + B_{2a}(L - z)\right)\left(\frac{dz}{dt}\right)^2. \quad (26)$$

3. Experimental device

The theoretical models developed in the previous section were tested using the experimental device shown in figure 4. It is essentially a transparent cylindrical tube made of acrylic plastic with diameter $2R = 0.150$ m and height $h = 1.50$ m, sealed at the bottom end and with a removable lid at the upper end. A yellow metric scale was fastened to the outer surface of the cylinder to make length measurements. The tube was filled with water from the upper side.

The actual sphere used was a table-tennis ball with radius $r = 0.0185$ m, filled up with different amounts of sand in order to vary its mass. An alluminum chain (a jewelry accessory) with diameter $D_C = 0.006$ m, length $L_C = 3.00$ m and total mass $M = 60.9$ g was coupled to the sphere through a perforation, acting at the same time as a seal to avoid sand losses, as can be seen in figure 5. The other end of the chain was fixed to the top cover of the device. The schematic of this assembly is shown in figure 6.

The fluid used in the experiments was water, at a temperature between 20 °C and 25 °C. In this temperature range, the dynamical viscosity of water is $\eta = (0.95 \pm 0.06) \times 10^{-3}$ kg m^{-1} s^{-1} and its density is $\rho = 998$ kg m^{-3} [1].

The experiments were performed for various mass values. The mass of the sphere was modified by adding or removing sand from its interior. The mass values considered were 25, 35 and 51.5 g, and the experiments were carried out three times with each value. In addition, measurements were made both with the sphere alone—using in this case a mass of 29 g—as well as with the chain alone. In each case, the sphere was released at the surface of the fluid and its motion was recorded using a standard smartphone with a 5MP camera at 30 frames per second. The camera was located at a distance of about 1.35 m from the tube and at a height of 0.75 m. Finally, the recorded videos were analysed using the software *Tracker 4.95* [18].

4. Results and discussion

In order to assess the suitability of the theoretical models of section 2, we compared the predictions of each one with the experimental observations realised with the device presented in section 3. To facilitate the analysis of results, the organisation of this section reflects the structure of section 2.

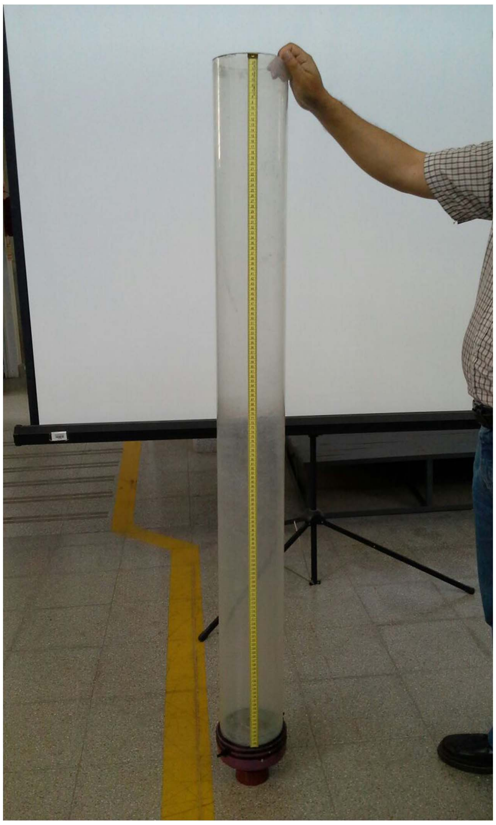

Figure 4. Image of the experimental device showing the acrylic tube with the yellow metric scale. To carry out the experiment, the cylinder was filled with water and the sphere-chain system shown in figure 5 was allowed to fall along the tube under the action of gravity.

The ordinary differential equations of the different models were solved for the parameters values and initial conditions of our experiment, by means of standard numerical integrators available for Python and Octave languages[5]. In what follows, we show and analyze our results.

4.1. Sphere alone

In figure 8, we show a typical experimental observation of the sphere's position, along with the predictions of the four models proposed to describe its motion. As can be seen, both model 1 (Stokes' viscous friction) and model 2 (Stokes' friction with Ladenburg's correction) show a similar behaviour and fit the experimental data well only for the initial instants (for a time of about a second). Thereafter, they diverge markedly from the measured values. This discrepancy can be attributed to the speed attained by the sphere by virtue of its dimensions and of the low viscosity of the fluid, which quickly leads the system to high Reynolds' numbers characteristic of the turbulent regime and not compatible with Stokes model

[5] In Octave (https://gnu.org/software/octave/), the *ode45* integrator was used. In Python (https://scipy.org/), numerical calculations were carried out using the *odeint* function of module *scipy.integrate.*

Figure 5. Image of the chain and sphere used, showing the coupling.

hypotesis [1–3]. Also, there is no appreciable difference between them, so it is apparent that the Ladenburg's correction do not improves the agreement between the theoretical predictions and the experimental values. However, models 3 and 4, which do take into account the turbulent character of the flow, correctly reproduces the trend in the measured data.

Figure 8 shows the experimental and numerical results obtained for the velocity of the sphere. It is observed experimentally that the sphere approaches a terminal speed. This fact is clearly highlighted by models 3 and 4, but this is not the case for the divergent models 1 and 2.

It can also be appreciated in figures 7 and 8 that the fit of model 4 (with variable drag coefficient) is only slightly better than the correlation exhibited by model 3 (with constant drag coefficient). However, the difference between both models is negligible.

Finally, we can see in figure 9 that the sphere traces a helical trajectory, as revealed by the horizontal component of the velocity of the sphere. This behaviour for objects falling inside fluids has been reported in previous investigations (see, for example [15]).

4.2. Sphere pulled by chain

In this subsection we discuss the results obtained for the system composed by the sphere and the chain. Figure 10 shows the measured values of the sphere's position for a typical

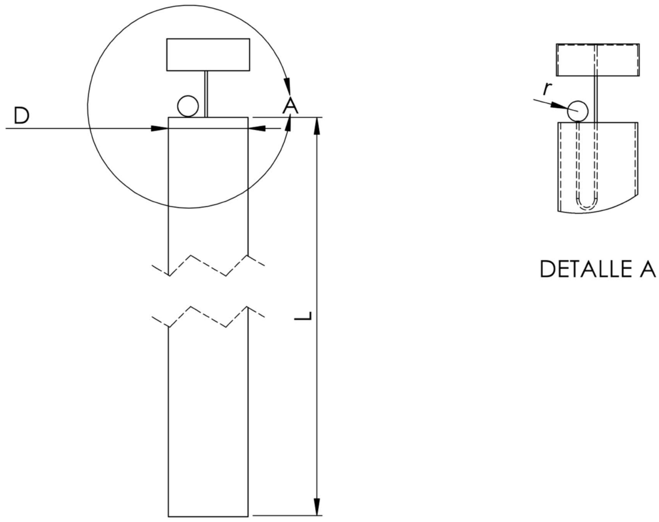

Figure 6. Detail of the coupling between chain, cover and sphere. When the sphere is released at the surface of the fluid, it is dragged by the section of the chain that hangs from it down to the bottom of the device.

experiment, along with the numerical results for each model. As in the case of the sphere alone, numerical predictions of models 3 and 4 show much better agreement with the experimental values than those of models 1 and 2, which only reproduce the measured data for a short time interval. In fact, when the system enters the regime of transition to turbulence ($Re \approx 10^3$), one can notice a growing gap between models based on Stokes' law and the experimental data, suggesting that these models are being applied outside its range of validity.

The free parameter used for the fit was, depending on the case, the coefficient of friction per unit lenght B_2 (in models 1 and 2) or the drag coefficient of the chain B_{2a} (in models 3

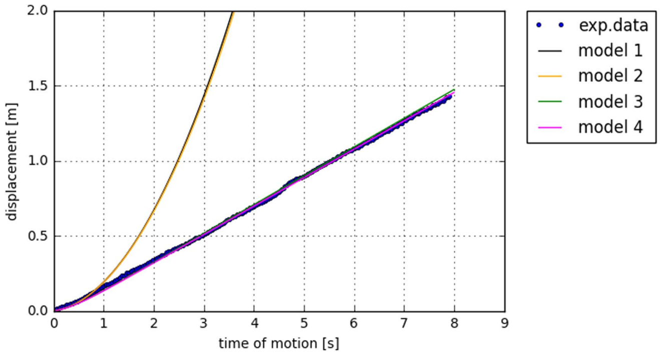

Figure 7. Position z of the sphere (without the chain) as a function of time t. Blue dots represent experimental data (the uncertainty in the measured values is of the order of the dot size, as calculated in the appendix). Black continuous line shows values predicted by model 1 (friction proportional to speed). Orange continuous line shows results for model 2 (friction proportional to speed plus correction by edge effect). Results for models 3 and 4, which include drag forces proportional to the square of the velocity, are indicated in green and magenta continuous lines, respectively.

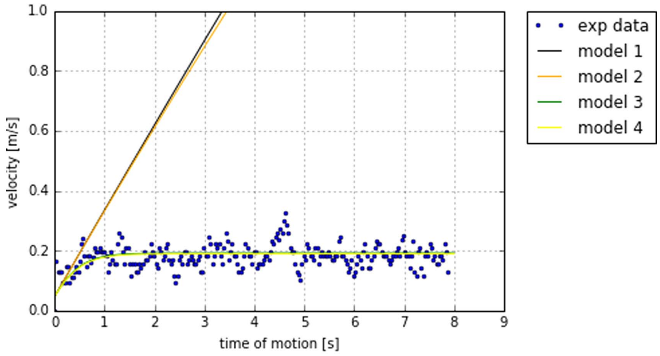

Figure 8. Vertical speed $\mathrm{d}z/\mathrm{d}t$ of the sphere (without the chain) as a function of time t. Experimental values are indicated by blue dots. Models 1 and 2 with friction proportional to speed and models 3 and 4 with friction proportional to the speed squared are represented by black, orange, green and yellow lines respectively.

and 4). In the case of models 1 and 2, no value of the coefficient of friction B_2 improved sensibly the fit to the experimental data. On the other hand, the value of the drag coefficient of the chain B_{2a}, which was the only free parameter in models 3 and 4, was estimated as 0.6 in order to achieve the best fit. This value was approximately constant in all the experiments performed with the different masses (25, 35 and 51.5 g) showing the consistence of the model.

In the study of the velocity of the sphere-chain system, no terminal velocity was experimentally observed. Figure 11 shows that the speed of the system decreases with time, and this trend is correctly captured by model 4 only. On the other hand, the difference between models 3 and 4 is much more noticeable here, and the benefit of incorporating the variable drag coefficient into the model is evident.

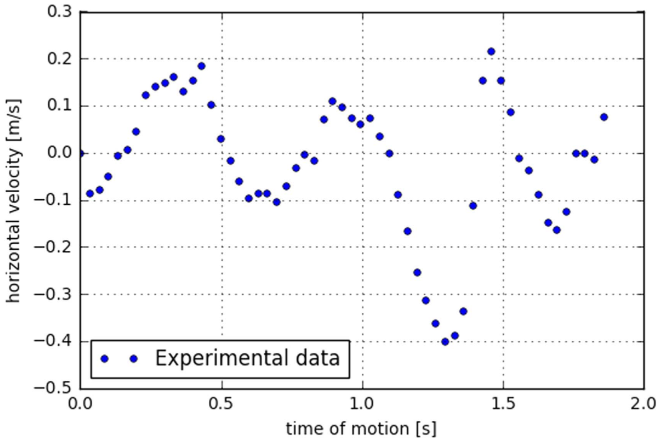

Figure 9. Horizontal velocity of the sphere alone as a function of time, which shows the horizontal projection of the sphere's helical motion as reported in previous works [15].

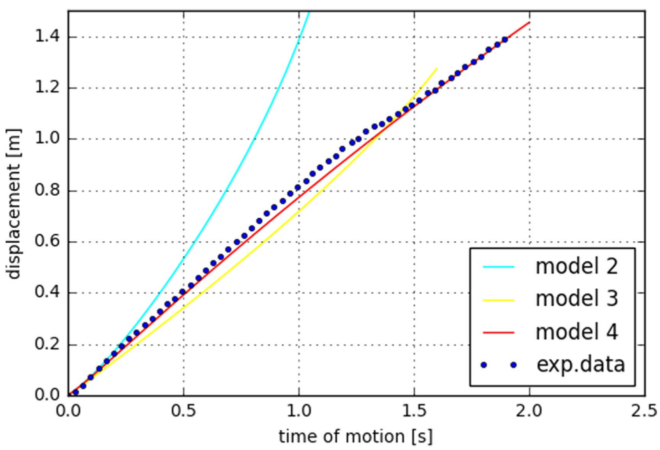

Figure 10. Position z of the sphere pulled by the chain as a function of time t, for a sphere of mass $m = 51.5$ g. Blue dots are experimental values (whose size represents the estimated uncertainty), while cyan, yellow and red continuous lines are the predicted values of models 2, 3 and 4, respectively. Results for model 1 are not shown, as its results are practically indistinguishable from those of model 2.

5. Conclusions

In this work we investigated a problem—similar to other typical ones covered in many textbooks—which integrates concepts of fluids and elementary mechanics from an theoretical, computational and experimental point of view. We have shown in a didactic context the construction of models of increasing complexity with the aim to address the model-building process at the undergraduate level, and to stress the importance of experimental validation. This integrated approach allows one to discuss in the classroom and in the

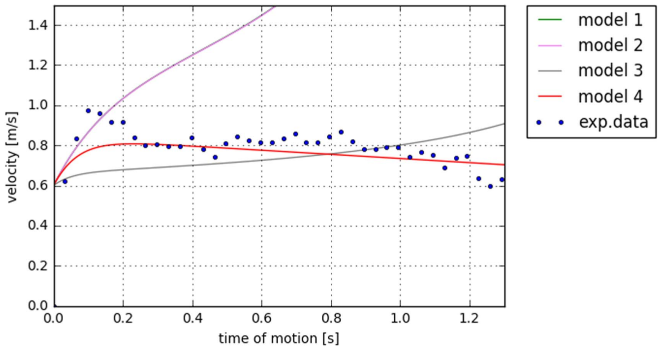

Figure 11. Vertical velocity dz/dt of the sphere pulled by chain as a function of time, for a sphere of mass $m = 51.5$ g.

laboratory the limitations and domains of application of a given mathematical model, conveying a deeper and more meaningful insight on the scientific activity. Also, by working with models without analytical solution, we can emphasise the importance of introducing a computational perspective into the undergraduate curriculum. The phenomenon investigated can suggest variations in many directions (for example by modifying objects' geometry, fluid characteristics, etc) and is amenable to be addressed without sophisticated technology.

Acknowledgments

We gratefully acknowledge the staff of the Engineering Lab and the Interactive Imaginary Museum of Universidad Nacional de General Sarmiento (UNGS) for providing us with materials, physical space and technical support. This work was carried out under project UNGS.IDEI 30/4077 'Uso de tecnologías de la información y la comunicación como apoyo a la formación de estudiantes de ciencias e ingeniería'. We also thankfully acknowledge Dr Rafael González (IDH-UNGS) for his careful review of the manuscript and for fruitful discussions.

Appendix. Calculation of the error in the position of the sphere

In addition to errors inherent to the accuracy of the measuring instruments used, two systematic errors were taken into account: parallax error and refraction error. A schematical representation of the two errors is shown in figure A1.

A.1. Parallax error

The parallax error appears since the measurements were made with a smartphone located at a distance of 1.35 m from the acrylic tube (whose radius is $R = 0.075$ m) and at a height of 0.75 m (half the height of the tube), and the sphere moves through the axis of symmetry of the cylindrical tube. In addition, the measurement scale was placed on the outer surface of the container. This type of error is generally taken into account as shown by the work of Sandoval *et al* [13], so we will not delve into more details here.

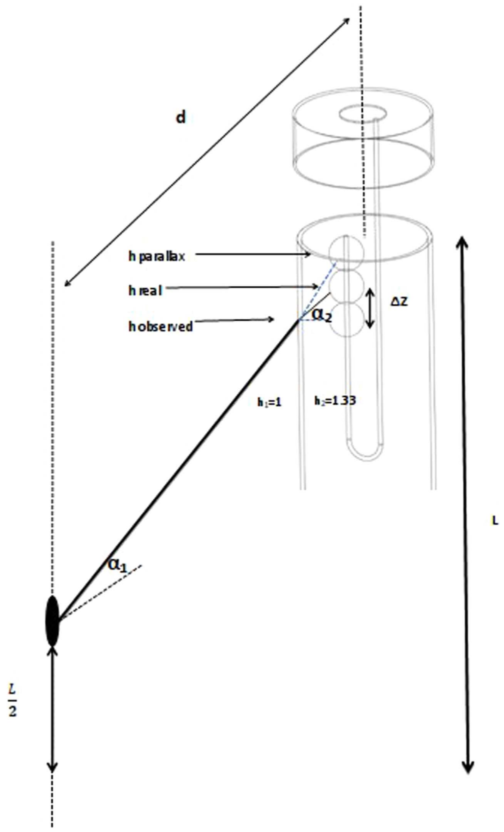

Figure A1. Schematic representation of the physical quantities involved in the determination of parallax and refraction errors.

A.2. Refraction error

Taking into account that the sphere is submerged in water (whose refraction index is approximately $h_2 = 1.33$) and that the tube has a certain radius, the observed position of the sphere is actually a virtual image of the sphere. The real position of the sphere is below the observed position. This phenomenon is shown in figure A1.

A.3. Systematic error in position considering parallax and refraction errors

For the following analysis, we assume the worst situation, i.e. when the sphere is located at one of the ends of the tube, which gives the maximum error in position.

If we consider that a beam of light exits from the sphere, when that beam passes from an optically denser medium (water, $h_2 = 1.33$) to air ($h_1 = 1.0$) the beam will change its direction as it crosses the interface between the media. If we take as a reference the normal to the lateral surface of the tube, the light beam will emerge from the sphere with an angle α_2 and will leave the tube with an angle α_1. The relationship between these angles is determined by Snell's law:

$$h_1 \sin(\alpha_1) = h_2 \sin(\alpha_2).$$

On the other hand, the angle is determined by the position of the camera and the length of the tube by the following expression:

$$\alpha_1 = \arctan\left(\frac{L/2}{d}\right),$$

where L represents the length of the tube and d the distance of the smartphone. In our experimental situation, $\alpha_1 \approxeq 29°$. A straightforward calculation using Snell's law gives $\alpha_2 = 21.41°$. Knowing the angle α_2, it is now possible to estimate the height error by parallax from

$$\Delta z = R\ \tan(\alpha_2)$$

which gives $\Delta z = 0.03$ m.

ORCID iDs

Horacio D Salomone https://orcid.org/0000-0003-2650-6723
Lisandro A Raviola https://orcid.org/0000-0002-7590-0543

References

[1] Mott R L 2014 *Applied Fluid Mechanics* 7th edn (London: Pearson) p 441
[2] Morrison F A 2013 *An Introduction to Fluid Mechanics* (Cambridge: Cambridge University Press) ch 8.1 p 601
[3] Streeter V L, Wylie E B and Bedford K W 1998 *Fluid Mechanics* 9th edn (New York: McGraw-Hill) ch 7.3
[4] Stokes G G 1880 *Collected Mathematical and Physical Papers* (Cambridge: Cambridge University Press) p 75
[5] Franklin A 1997 Millikan's oil-drop experiments *Chem. Educator* **2** 1
[6] Viswanath D S *et al* 2007 *Viscosity of Liquids. Theory, Estimation, Experiment, and Data* (Dordrecht, NL: Springer)
[7] Nashol D 1965 Measuring viscosity by Stokes's law *Am. J. Phys.* **33** 657
[8] Wray E M 1977 Stokes' law revisited *Phys. Educ.* **12** 300
[9] Greenwood M S *et al* 1986 Using the Atwood machine to study Stokes' law *Am. J. Phys.* **54** 904
[10] Lindgren E R 1988 Comments on using the Atwood machine to study Stokes' law *Am. J. Phys.* **56** 940
[11] Auerbach D 1988 Some limits to Stokes' law *Am. J. Phys.* **56** 850
[12] Owen J P and Ryu W S 2005 The effects of linear and quadratic drag on falling spheres: an undergraduate laboratory *Eur. J. Phys.* **26** 1085–91
[13] Sandoval C, Caram J and Salinas J 2009 The misleading simplicity of 'Stokes method' for viscosity measurement *Rev. Bras. Ens. Fís.* **31** 4310
[14] Fernández Cruz R *et al* 2014 Puntualizaciones en las aplicaciones didácticas de la ley de Stokes *Lat. Am. J. Phys. Educ.* **8** 126
[15] Lee C B *et al* 2013 Experimental investigation of freely falling thin disks: 2. Transition of three-dimensional motion from zigzag to spiral *J. Fluid Mech.* **732** 77–104
[16] Ladenburg R 1907 *Ann. Phys.* **22** 287
Ladenburg R 1907 *Ann. Phys.* **23** 447
[17] Francis A W 1933 Wall effect in falling ball method for viscosity *Physics* **4** 403
[18] Brown D and Cox A J 2009 Innovative uses of video analysis *Phys. Teach.* **47** 145